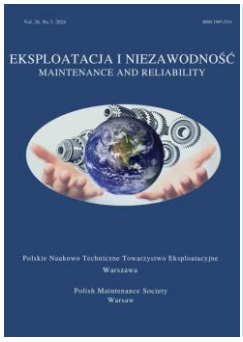

Eksploatacja i Niezawodnosc – Maintenance and Reliability

Volume 26 (2024), Issue 3

journal homepage: http://www.ein.org.pl

Article citation info:
Zhou Z, Chen W, Ma J, Advanced Sparse Filtering-Based Domain Adaptation for Fault Diagnosis in Variable Working Conditions, Eksploatacja i Niezawodnosc – Maintenance and Reliability 2024: 26(3) http://doi.org/10.17531/ein/187889

Advanced Sparse Filtering-Based Domain Adaptation for Fault Diagnosis in Variable Working Conditions

Indexed by: Web of Science Group

Ziyou Zhou[a], Wenhua Chen[a,*], Jian feng Ma[a]

[a] National and Local Joint Engineering Research Center of Reliability Analysis and Testing for Mechanical and Electrical Products, Zhejiang Sci-Tech University, China

Highlights

- Incorporating normalization and cosine penalty into sparse filtering enhances cross-domain feature extraction consistency.
- Integrating Bootstrap with maximum mean discrepancy improves domain difference assessment accuracy.
- The proposed method effectively addresses variable working condition fault diagnosis challenges.

Abstract

Traditional domain adaptation (DA) methods often encounter challenges with cross-domain feature extraction and the precise assessment of domain differences. To overcome these limitations, we introduce the Enhanced Sparse Filtering-Based Domain Adaptation (ESFBDA) method. This method distinguishes itself by enhancing sparse filtering (SF) with the integration of row-column normalization and a cosine penalty, specifically designed to minimize feature loss—a critical issue in existing DA techniques. Additionally, we employ Bootstrap resampling to refine domain distribution alignment, a novel step that boosts feature similarity and effectiveness in DA. This integrated approach ensures more accurate feature extraction, which is crucial for the classifier's fault detection capability. In our study, through two distinct experiments on Electro-Hydrostatic Actuator (EHA) internal leakage and bearing fault diagnosis, the ESFBDA method demonstrated remarkable accuracy, significantly surpassing traditional approaches and showcasing its robust applicability across varied diagnostic scenarios.

Keywords
domain adaptation, fault diagnosis, variable working conditions, sparse filtering

1. Introduction

Deep learning-based diagnostic methods typically assume uniform working conditions for both training and testing data [2, 17, 18, 35]. However, in real-world scenarios, variable working conditions can significantly impact diagnostic performance. Thus, addressing variable working conditions fault diagnosis is crucial.

Domain adaptation (DA) has become a common solution for address the issue of variable condition fault diagnosis [15, 19, 22, 26]. For example, An et al. [1] proposed a domain adaptation network based on contrastive learning (DACL), aimed at enhancing fault diagnosis under variable working conditions. Ding et al. [8] introduced a deep unbalanced domain adaptation (DUDA) framework for bearing fault diagnosis.

The effectiveness of DA in fault diagnosis under variable working conditions depends on two key aspects [8]. Firstly, it is essential to extract features that remain consistent across different conditions. Sparse filtering (SF), an unsupervised technique, is commonly used for this type of feature extraction in variable condition fault diagnosis [30]. For instance, Ji et al. [13] introduced a parallel SF-based DA approach with an extra

(*) Corresponding author.
E-mail addresses: Z. Zhou (ORCID: 0000-0002-0402-6537) zhouziyou1995@gmail.com, W. Chen chenwh@zstu.edu.cn, J.Ma alickyeti@163.com,

normalization step, while Zhang and Yang developed a reconstruction-oriented orthogonal SF-based technique to address redundant feature extraction. The existing normalization process in SF may have limitations when dealing with complex data structures. Particularly in high-dimensional and diverse datasets, this approach can sometimes overemphasize uniform standardization, potentially leading to the loss of key features or an inability to capture subtle data variations, thus affecting overall model performance.

The second critical factor for DA in fault diagnosis is the accuracy in assessing domain discrepancies[12, 16]. Maximum mean discrepancy (MMD) is widely used for this purpose in SF-based DA methods, notably for aligning features from the source domain with those in the target domain [5, 20, 24]. Prominent implementations of MMD include the hierarchical MMD by Sebastian et al. [21] , which has shown effectiveness in various bearing fault diagnoses, particularly under notable speed variations. Zhang et al. [29] developed the generalized normalized MMD, an innovative feature-learning approach designed for more unstable scenarios. However, when the data points are insufficient to represent the true distribution, or there are substantial differences between domains, the estimated MMD values may become inaccurate or unstable.

To mitigate these challenges, this study unveils the enhanced sparse filtering-based domain adaptation (ESFBDA) strategy. ESFBDA incorporates bidirectional normalization and a cosine similarity-based penalty term within SF and employs Bootstrap resampling in MMD estimation. This refined strategy aims to preserve essential features for classification; reduce erroneous redundancy assumptions; and improve the accuracy and stability of MMD estimations in various domain discrepancy scenarios. It is worth mentioning that paper [32] introduces a supervised contrastive learning-based approach for rolling bearing fault diagnosis, distinguishing it from our method through different DA and feature extraction techniques. Paper [31] introduces a digital twin-driven approach for fault diagnosis with simulated data, whereas our method uniquely enhances DA through advanced SF. The ESFBDA method is uniquely designed to enhance diagnostic accuracy by improving feature extraction consistency and DA precision. By integrating advanced normalization techniques and employing Bootstrap resampling in conjunction with MMD, our approach addresses critical gaps in existing DA methodologies. These innovations enable the ESFBDA method to effectively overcome the challenges of variable working conditions, setting a new standard for fault diagnosis accuracy and reliability.

The main contributions of this work are as follows:

1. We propose a novel enhanced SF approach by integrating row-column normalization and a cosine penalty. This enhancement aims to significantly reduce feature loss compared to traditional SF methods, thereby optimizing the feature extraction process for more accurate fault diagnosis.

2. We introduce an innovative approach by incorporating Bootstrap resampling into the MMD algorithm, thereby enhancing the accuracy of domain discrepancy assessments, particularly effective in scenarios with limited sample sizes.

3. Experiments were performed under variable working conditions and internal leakage scenarios in EHA systems to validate the effectiveness of the proposed ESFBDA method. The results consistently demonstrate its efficacy and reliability, outperforming established methods and conventional SF-based DA strategies.

The structure of this paper is as follows: Section 2 offers an overview of SF and MMD. Section 3 details the implementation of the ESFBDA. Section 4 validates the ESFBDA method through diagnostic tests for internal leakage faults in Electro-Hydrostatic Actuators (EHA) under varying conditions. Finally, Section 5 summarizes our findings and conclusions.

2. Theoretical Background

Before introducing the proposed ESFBDA method, an overview of some foundational theories relevant to ESFBDA is presented in this section. This includes SF and MMD.

2.1. Sparse Filtering

Standard SF is an efficient unsupervised feature learning algorithm [28]. Suppose there exists the following linear mapping:

$$\mathrm{f}_j^i = \mathrm{W}_j^T \mathrm{x}^{\mathrm{i}} \tag{1}$$

where the $x^i \in R^{N\times 1}$ is a training sample, $\boldsymbol{W} \in R^{N\times L}$ is weight matrix, $\boldsymbol{f}_j{}^i \in R^{L\times 1}$ corresponds to the jth feature of the i sample.

In this case, these normalized features can be optimized. An l_1-norm penalty is applied to enforce sparsity. For a dataset with M samples, the objective function of SF can be represented as follows:

$$J_{sp}(\mathrm{W}) = \underset{W}{minimize} \sum_{i=1}^{M} \left\| \hat{\mathrm{f}}^i \right\|_1 = \sum_{i=1}^{M} \left\| \frac{\tilde{f}^i}{\|\tilde{f}^i\|_2} \right\|_1 \quad (2)$$

where, M is the total number of samples, $\hat{f}^i$ is the feature vector for the i^{th} sample, $\tilde{f}^i$ is the normalized version of $\hat{f}^i$ where normalization is done by the l_1 norm across features for each sample, and $\|\cdot\|_1$ denotes the l_1 norm that enforces sparsity.

2.2. Maximum Mean Discrepancy

Consider two distributions D_S and D_T, and our goal is to compute the MMD between them.

D_S=$\{x_{S1}, x_{S2}, \ldots x_{Sn}\}$ and D_T=$\{x_{T1}, x_{T2}, \ldots x_{Tm}\}$, where n and m are the sizes of the respective sample sets.

The formula for MMD described as:

$$\mathrm{MMD}^2(D_S, D_T) = \left\| \frac{1}{n}\sum_{i=1}^{n} \phi(x_{Si}) - \frac{1}{m}\sum_{j=1}^{m} \phi(x_{Tj}) \right\|^2 \quad (3)$$

where ϕ is a mapping function that maps samples into a feature space.

3. The Proposed Method

In this section, a novel fault diagnosis method in variable working conditions, ESFBDA, is introduced. The structure of this method is depicted in Fig. 1 and is comprised of three main steps: data preprocessing in the first step, the construction of the objective function in the second step, and the construction of the classifier in the third step.

3.1. Data Preprocessing

Assuming the collected signal is represented as $g[n]$, where n = 0, 1, 2, …, N-1, the signal is subsequently subjected to Short-Time Fourier Transform (STFT).

Following the procedure outlined in[10] , the time-frequency signal $x[m, k]$ is computed as follows:

$$x[m,k] = \sum_{n=0}^{M-1} X\,[mR+n] e^{-j2\pi kn/N} \quad (4)$$

where $x[m, k]$ represents the signal strength at frequency k within the m-th time window, M is the window length, and R is the step size between windows.

Subsequently, normalization of the amplitude of the frequency-domain signal is performed. This step ensures uniform amplitude ranges across different signals, facilitating subsequent feature extraction, comparison, and analysis.

$$X[m,k] = \frac{x[m,k]}{A_{\max}} \quad (5)$$

where $A_{\max}$ represents the maximum amplitude of the time-frequency signal, and $X[m, k]$ represents the amplitude of the normalized time-frequency signal.

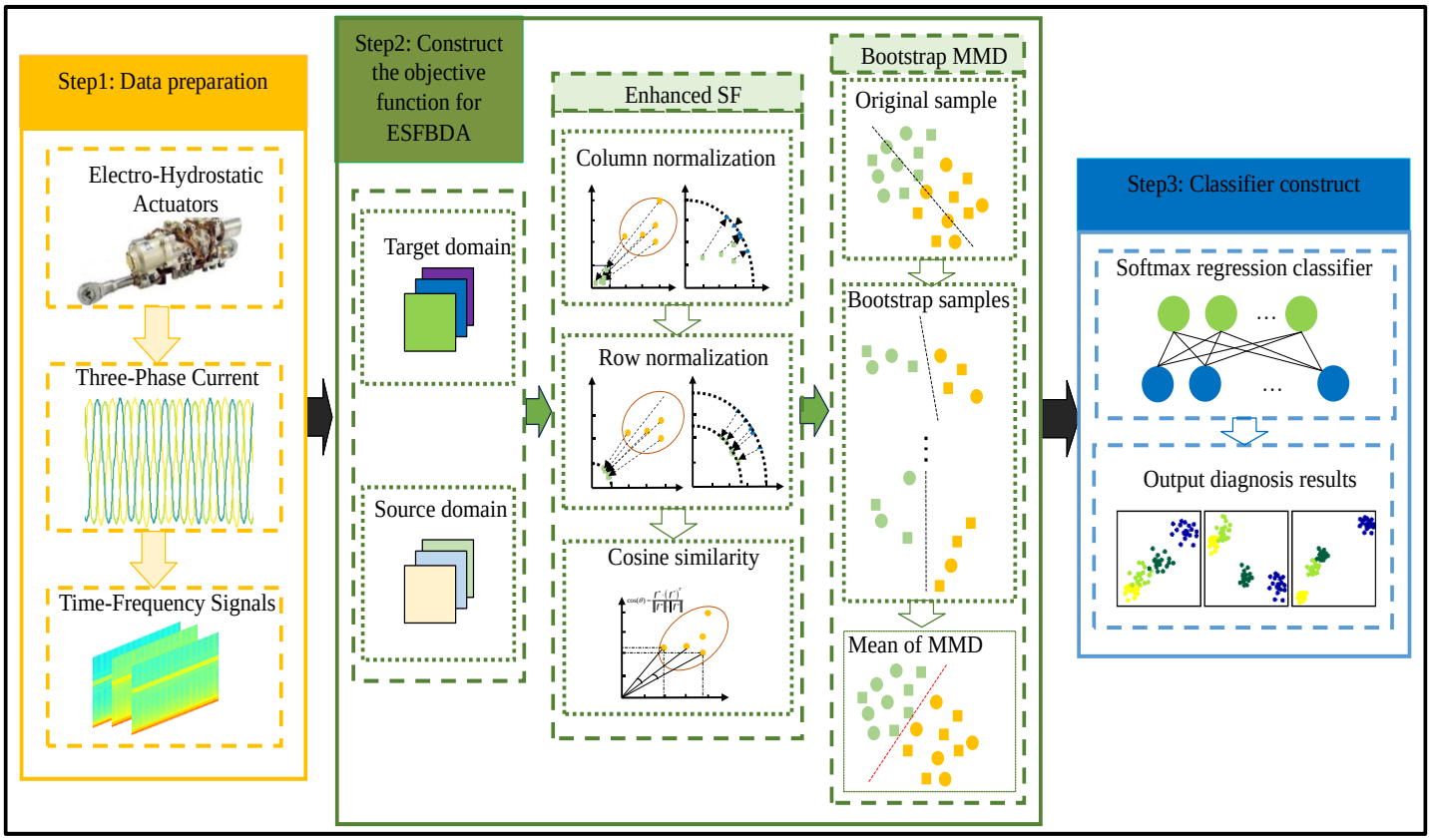

Fig. 1. The framework of the proposed method.

3.2. Construct the Objective Function for ESFBDA

3.2.1. Enhanced Sparse Filtering

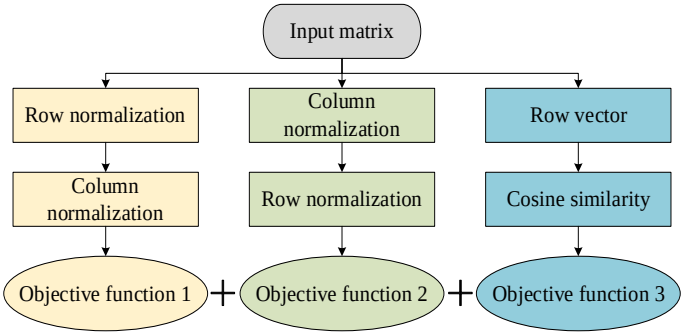

Fig. 2. Schematic of the enhanced SF method.

As shown in Fig. 2，Enhanced SF builds upon existing SF technology by introducing an additional normalization item and a similarity penalty item in different directions. The normalization item maps features onto a unit l_2 norm circle, preserving key features and optimizing activation values, crucial for handling features of varying sizes. The cosine similarity penalty item maintains feature diversity and uniqueness by penalizing similarity among basis vectors in feature space, encouraging the selection of both relevant and varied features.

Assuming data preprocessing yields a time-frequency signal X, it contains two similar yet differently distributed components: the source domain D_S and the target domain D_T. $S=[(x_1^s, y_1^s),(x_2^s, y_1^s)\ldots(x_{ns}^s, y_{ns}^s)]\sim(D_S)^{ns}$ denotes the labeled source domain dataset, and $T=[(x_1^t, x_2^t \ldots x_{nt}^t) \sim(D_T)^{nt}$ represents the unlabeled target domain dataset.

As shown in Fig. 3, first, normalize all columns using the l_2-norm, mapping the feature values to the unit l_2-norm sphere, so that their squared activation values become 1:

$$\hat{\mathrm{f}}^i = \frac{\mathrm{f}^i}{\|\mathrm{f}^i\|_2} \tag{6}$$

Then, normalize all rows equivalently using the l_2-norm activation:

$$\tilde{\mathrm{f}}_j = \frac{\hat{\mathrm{f}}_j}{\|\hat{\mathrm{f}}_j\|_2} \tag{7}$$

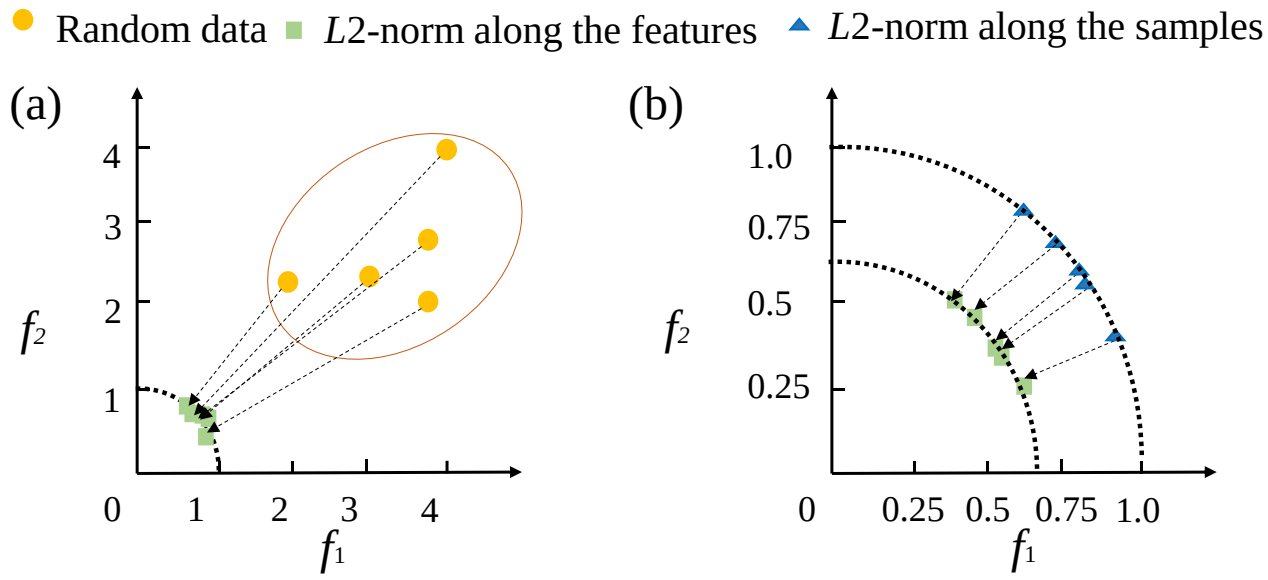

Fig. 3. Additional normalization term of enhanced SF; (a) Column normalization, (b) Row normalization.

Afterwards, utilize l_1-norm regularization to optimize the computed features, with the objective function for this direction being:

$$J_{rp}(\mathrm{W}) = \underset{W}{minimize} \sum_{i=1}^{N} \|\tilde{\mathrm{f}}_j\|_1 = \sum_{i=1}^{N} \left\| \frac{\hat{\mathrm{f}}_j}{\|\hat{\mathrm{f}}_j\|_2} \right\|_1 \tag{8}$$

Let $sim(\boldsymbol{f}^u, \boldsymbol{f}^v)$ represent the similarity matrix among all basis vectors in the weight matrix $\boldsymbol{W}$. The following form for the similarity penalty term can be employed.

$$J_{sim}(\mathrm{W}) = \alpha \sum_{u=1}^{M-1} \sum_{v=u+1}^{M} (1 - sim(\mathrm{f}^u, \mathrm{f}^v)) \tag{9}$$

where $\boldsymbol{f}^u$ and $\boldsymbol{f}^v$ are the u and v rows of matrix $\boldsymbol{W}$.

As shown in Fig. 4, using cosine similarity to measure the similarity between $\boldsymbol{f}^u$ and $\boldsymbol{f}^v$.

$$sim(\mathrm{f}^u, \mathrm{f}^v) = cos(\mathrm{f}^u, \mathrm{f}^v) \tag{10}$$

When two basis vectors are more similar, the cosine similarity approaches 1. When they are orthogonal to each other, the cosine similarity approaches 0. And when they are completely dissimilar, the cosine similarity approaches -1.

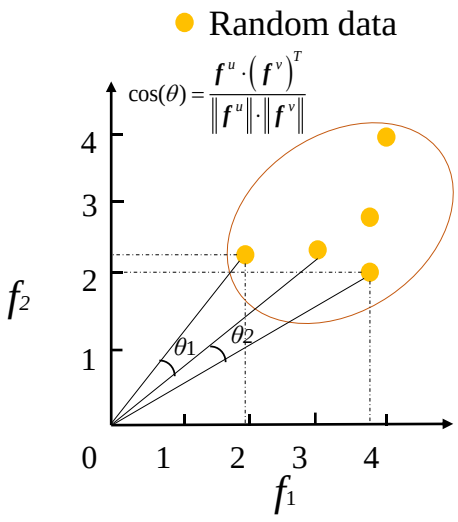

Fig. 4. Similarity penalty term of ESFBDA.

The final objective function for enhanced SF is obtained by integrating Eq. (2), (8) and (9) as follows:

$$J_{srps}(\mathrm{W}) = J_{sp}(\mathrm{W}) + \lambda J_{rp}(\mathrm{W}) + \alpha J_{sim}(\mathrm{W}) = \sum_{i=1}^{M} \left\| \frac{\tilde{f}_j}{\|\tilde{f}_j\|_2} \right\|_1 + \lambda \sum_{i=1}^{N} \left\| \frac{\tilde{f}^i}{\|\tilde{f}^i\|_2} \right\|_1 + \alpha \sum_{u=1}^{M-1} \sum_{v=u+1}^{M} (1 - \mathrm{sim}(\mathrm{f}^u, \mathrm{f}^v)) \quad (11)$$

where $\lambda \geq 0$ determines the weight between these two terms, α is a regularization parameter used to control the strength of the similarity penalty.

The innovative aspect of Enhanced SF lies in its sophisticated approach to addressing the challenges of fault diagnosis under variable working conditions, where traditional SF techniques may fall short. The key innovations of Enhanced SF include the integration of bidirectional normalization and a cosine similarity penalty. This combination aims to preserve essential features while minimizing feature loss that often occurs with conventional SF methods. Bidirectional normalization ensures that features are scaled appropriately, both row-wise and column-wise, to maintain their relative importance and to facilitate a more consistent feature extraction across different domains. The cosine similarity penalty discourages redundancy by penalizing similarity among features, encouraging the selection of diverse and informative features.

Compared to traditional SF technology, which primarily focuses on feature extraction without explicitly addressing the issue of feature redundancy or the need for feature consistency across domains, Enhanced SF introduces mechanisms to ensure that the extracted features are both relevant and varied, enhancing the model's ability to generalize across different working conditions. This is crucial for fault diagnosis applications where the operational conditions can vary widely, and the ability to accurately diagnose faults under such conditions is essential for maintaining system reliability and performance.

3.2.2. MMD with Bootstrap Resampling

Additionally, Bootstrap resampling into MMD, where multiple new datasets are created by randomly selecting data points with replacements from the original data. MMD is then computed for each of these resampled datasets, resulting in a distribution of MMD values. The algorithm schematic is depicted in Fig. 5.

The specific steps are as follows:

Step 1: Conduct Bootstrap sampling by independently drawing samples with replacement from D_S and D_T, constructing new sample sets $S_{\text{bootstrap}}$ and $T_{\text{bootstrap}}$.

Step 2: For each Bootstrap sample set $S_{\text{bootstrap}}$ and $T_{\text{bootstrap}}$, compute the corresponding MMD value:

$$\mathrm{MMD}^2_{\text{bootstrap}}(D_S, D_T) = \left\| \frac{1}{n} \sum_{i=1}^{n} \phi(S_{\text{bootstrap},i}) - \frac{1}{m} \sum_{j=1}^{m} \phi(T_{\text{bootstrap},j}) \right\|^2 \quad (12)$$

Step 3: Increase the bootstrap iterations incrementally, assessing the MMD estimate's variance after each set. Cease iterations when the variance change between sets falls below a pre-determined, small threshold value, such as 0.1% of the initial variance. This threshold ensures sufficient stability in the MMD estimate without unnecessary computation.

Step4: From the distribution of bootstrap MMD values, compute the confidence intervals (95% CI):

$$L_{mmd}(\mathrm{W}) = [\hat{\mu}_{\mathrm{MMD}} - 1.96 \times \frac{\hat{\sigma}_{\mathrm{MMD}}}{\sqrt{1000}}, \hat{\mu}_{\mathrm{MMD}} + 1.96 \times \frac{\hat{\sigma}_{\mathrm{MMD}}}{\sqrt{1000}}] \quad (13)$$

where $\hat{\mu}_{\mathrm{MMD}}$ is the mean of MMD values and $\hat{\sigma}_{\mathrm{MMD}}$ is the standard deviation.

It is evident that if the confidence interval is larger, it implies higher uncertainty in the estimation of MMD, leading to a less precise assessment of differences between probability distributions. Conversely, when a smaller confidence interval is used, greater confidence in the stability of the estimation is achieved, indicating smaller disparities between the distributions.

By combining the enhanced SF term with the domain distribution discrepancy alignment term, the following

objective function can be obtained.

$$L(\mathrm{W}) = L_{srps}(\mathrm{W}) + \beta L_{mmd}(\mathrm{W}) \quad (14)$$

where the tradeoff between two terms is controlled by $\beta > 0$.

Ultimately, by solving Eq. (1) under the constraints of the objective function Eq. (14), the feature matrix is obtained.

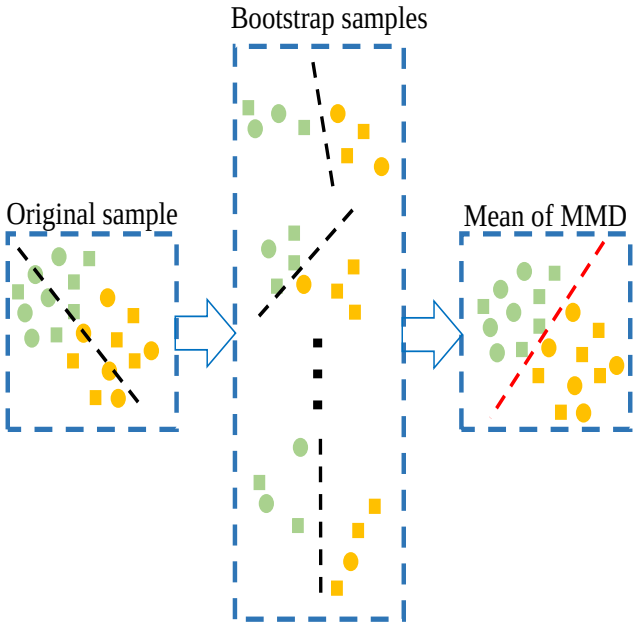

Fig. 5. The algorithm schematic for Bootstrap resampling into MMD.

3.3. Fault Diagnosis

In the proposed method, the softmax regression classifier is employed due to its proficiency in handling multi-class classification, essential for accurate fault diagnosis across various conditions [7, 14, 27]. This classifier, with its probabilistic output, offers interpretability in results, providing both classifications and their confidence levels. Its compatibility with the feature set extracted through the ESFBDA method ensures effective and accurate fault identification under various working conditions.

The training data T_r sourced from the dataset is utilized to train the softmax regression classifier. Subsequently, the efficacy of the softmax regression classifier is assessed using the test data T_e that encompasses all categories.

$$T_r = Z(\mathrm{W} \cdot \mathrm{M}_S)T_e = Z(\mathrm{W} \cdot \mathrm{M}_T) \quad (15)$$

where Z represents *Z-score* normalization, and $\boldsymbol{W}$ is the weight matrix learned.

Furthermore, the trained softmax regression classifier is utilized to diagnose samples from the target dataset.

In conclusion, the proposed algorithm can be summarized as an algorithm table.

Algorithm: ESFBDA

Input: Sample set X, including the source domain data X_S and the target domain data X_T, source labels Y_S, weight parameter λ, regularization parameter α, and β.
Output: Predicted labels for each test sample in the target domain X_T.

Train:
1. Calculate the column-wise l_2-norm of data X using Eq. (6), followed by the row-wise l_2-norm of the obtained result.
2. Calculate the row-wise l_2-norm of data X, followed by the column-wise l_2-norm of the obtained result.
3. Apply the l_1-norm using Eq. (7) to the features obtained in steps 1 and 2.
4. Compute the similarity between all base vectors in X.
5. Calculate the similarity penalty term based on the computed similarities using Eq. (9).
6. Calculate the bootstrap MMD value of X according to Eq. (13).
7. Integrate the results from steps 3 and 6, constructing the final objective function based on Eq. (11).
8. Employ X_S and X_T as the input data for ESFBDA, and minimize the objective function from step 8 to obtain the weighted matrix $\boldsymbol{W}$.
9. Compute training data T_r and test data T_e for the softmax classifier.

Classify:
Employ the softmax classifier to predict labels Y_T for unlabeled target data X_T.

4. Experiment Results and Analysis

4.1. Case 1: EHA Internal Leakage Fault Diagnosis

4.1.1. Data Preparation

To ascertain the efficacy of the ESFBDA method in variable working condition fault diagnosis, an EHA internal leakage test bench was constructed, as shown in Fig. 6.

The motor was then operated at speeds of 72,000 rpm, 144,000 rpm, and 216,000 rpm, respectively, while achieve oil discharge rates of 3 mL, 5 mL, and 8 mL under different speeds. These were respectively calibrated as mild, moderate, and severe internal leakages at each speed.

Therefore, in this experimental study, three different EHA operating speeds were set (72,000 rpm, 144,000 rpm, 216,000 rpm), designated as conditions 1, 2, and 3, respectively. Under these conditions, four levels of leakage faults (labeled A, B, C, D) were introduced, where A represents no leakage, and the severity increases from A to D.

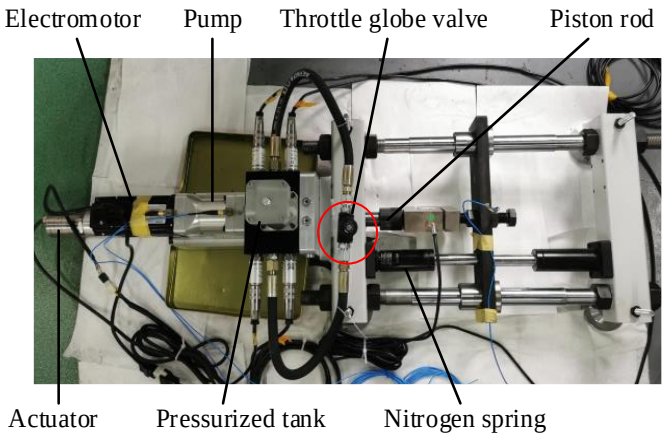

Fig. 6. Simulation test bench for internal leakage.

Six variable working conditions fault diagnosis experiments were designed, ranging from a single-source domain to a single-target domain, and detailed information for each condition is presented in Table 1. In each DA task, for example, case 1-2 signifies that dataset 1 was used as the source domain for feature learning, and health condition diagnosis was performed on samples from the target domain 2.

Table 1. Description of planetary leakage dataset (single source domain).

Transfer Task	Source Domain (rpm)	Target Domain (rpm)	Source Samples	Target Samples	Health Conditions
1-2	72000	144000	400	80	A, B, C, D
1-3	72000	216000	400	80	
2-1	144000	72000	400	80	
2-3	144000	216000	400	80	
3-1	216000	72000	400	80	
3-2	216000	144000	400	80	

Furthermore, experiments were also conducted to select two source domains to predict the health condition of a target domain. There are three tasks in this experiment: 12-3, 13-2, and 23-1. Specific details of the experiment are presented in Table 2.

Table 2. Description of planetary leakage dataset (double-source domains).

Transfer Task	Source Domain (rpm)	Target Domain (rpm)	Source Samples	Target Samples	Health Conditions
12-3	72000&144000	216000	200×2	80	A, B, C, D
13-2	72000&216000	144000	200×2	80	
23-1	144000&216000	72000	200×2	80	

The signals collected by the sensors were input into a data acquisition instrument, and the sampling frequency was set at 25600 Hz. In the experiment, each state comprised 20 samples, with each sample containing 51200 data points.

First, under three distinct operating conditions, the three-phase current signals of the servo motor were collected, as illustrated in Fig. 7. These signals serve as a comprehensive representation of the system's electrical behavior during its operation.

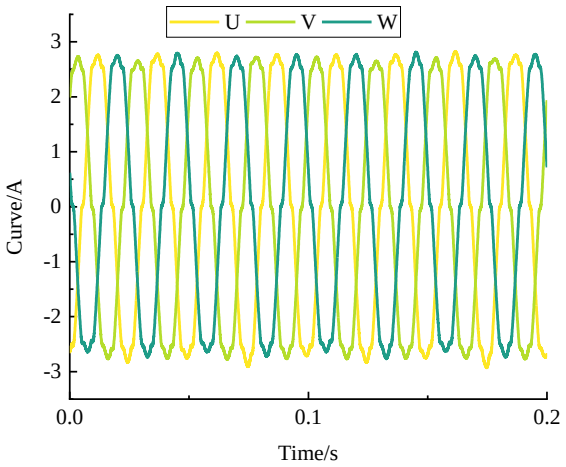

Fig. 7. Schematic representation of three-phase current signals from the servo motor; 'u,' 'v,' and 'w' represent the phase currents of the EHA motor.

Furthermore, the peak values of the three-phase current waveforms were separately extracted. As depicted in Fig. 8, this gives us a time-series curve showing the evolution of the three-phase current peaks. It's an essential step because these peak values can provide insights into the motor's operational dynamics under different conditions.

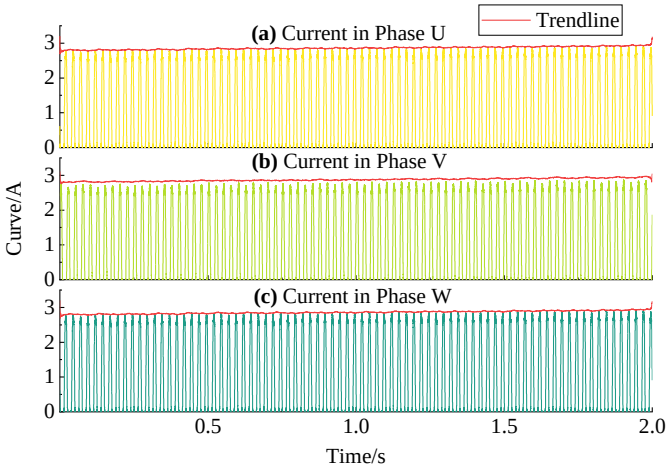

Fig. 8. Extraction of peak values from three-phase current signals.

Fig. 9 presents the envelope lines of current peak values for various leakage amounts under a particular operating condition. An interesting observation from the Fig. 9 is the subtle changes in the current peaks' progression, suggesting different health conditions of the system. However, discerning these variations merely by visual inspection proves challenging, emphasizing the need for more sophisticated analysis techniques to precisely identify different system health statuses.

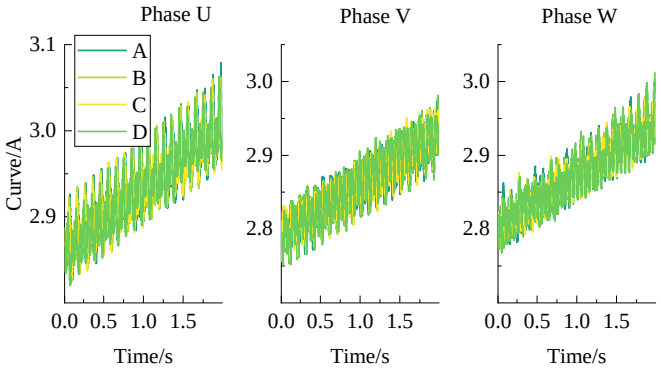

Fig. 9. Peak current signal for different leakage levels under a specific operating condition.

The peak current signal was subjected to STFT to extract time-frequency features. As shown in Fig. 10, the STFT analysis results of the peak current signal for a sample under healthy conditions at 72000 rpm were presented in the form of a heat map. The features extracted using the STFT method are quite pronounced. Consequently, the time-frequency analysis results of the current peak signal are utilized as input for subsequent analysis.

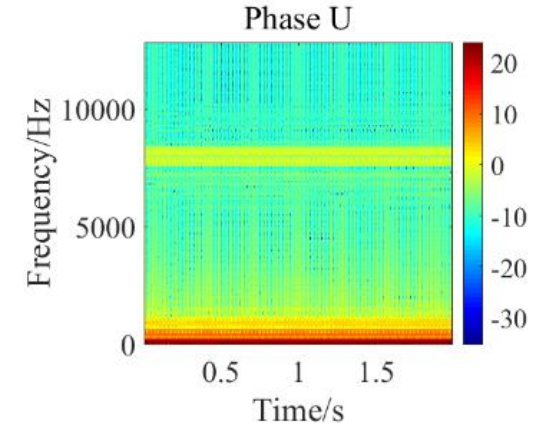

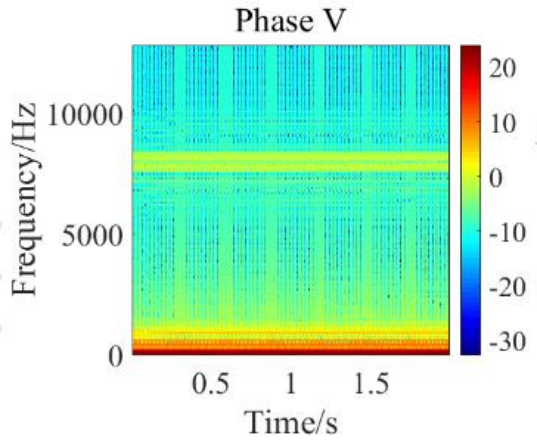

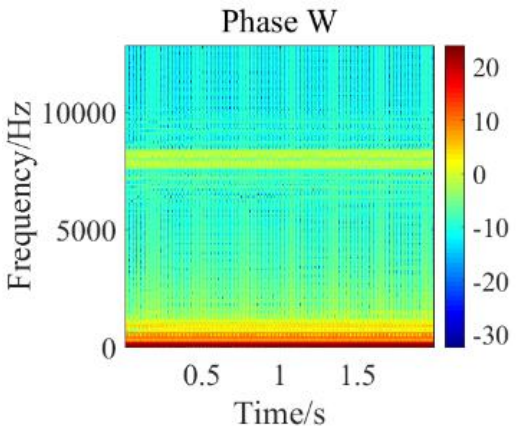

Fig. 10. Time-frequency maps of three-phase current.

4.1.2. Comparison Methods and Parameter Selection

To accentuate the benefits of the method we've proposed for diagnosing EHA leakage faults across diverse scenarios, a series of comparative experiments were initially set up to highlight the innovative aspects of our approach. This was complemented by juxtaposing our method against other avant-garde techniques in variable working conditions diagnostics. (Detailed methods follow).

1. Sparse filtering domain adaptation (SFDA): A foundational method that combines traditional MMD for DA with unmodified SF for feature extraction. SFDA serves as a baseline, allowing us to assess the fundamental effectiveness of SF in conjunction with standard MMD in fault diagnosis.

2. Sparse Filtering with Bootstrap Maximum Mean Discrepancy (SFBDA): Enhances DA through the use of MMD optimized by Bootstrap resampling, followed by feature extraction employing conventional SF techniques. This method highlights the impact of Bootstrap optimization on the accuracy of MMD calculations, thereby potentially improving DA effectiveness without altering the SF component.

3. Reconstruction sparse filtering domain adaptation (RSFDA) [34]: Utilizes MMD for DA while incorporating soft reconstruction penalties (SRP) into the SF process for feature extraction. RFSFDA explores the potential of SRP to enhance feature representation by adding reconstruction constraints, offering an advanced approach to leveraging SF for improved DA.

4. $\mathcal{A}$ −distance and sparse filtering domain adaptation (ASFDA) [11]: Employs $\mathcal{A}$ -distance to measure the discrepancy between domains, combined with SF for feature extraction. ASFDA investigates the utility of $\mathcal{A}$ -distance as an alternative metric for quantifying domain differences, aiming to complement SF in the domain adaptation process.

5. l_1/l_2− norm distance and sparse filtering domain adaptation l_1/l_2-SFDA [25]: Features an enhanced SF network that applies l_1/l_2-norm adjustments for feature extraction, with MMD assessing domain discrepancies. l_1/l_2-SFDA examines the benefits of combining norm-based modifications with SF to enhance DA, focusing on the advantages of parallel positive-side normalization.

6. Enhanced sparse filtering with maximum classifier discrepancy (SFMCD)[3]: Integrates the Wasserstein distance for minimizing domain differences, paired with SF for feature extraction. SFMCD represents an innovative approach to domain adaptation, leveraging advanced distance measures to refine the alignment between source and target domains, thereby potentially enhancing the effectiveness of SF.

In our comparative analysis, SFDA and SFBDA serve to evaluate the core improvements to SF and MMD, establishing a baseline for the effectiveness of traditional DA techniques. Conversely, RSFDA, ASFDA, l_1/l_2-SFDA, and SFMCD are employed as benchmarks against other state-of-the-art domain adaptation methods in variable working conditions diagnostics, showcasing a range of optimized sparse filtering-based approaches. This comprehensive comparison aims to underline the superiority and innovation of our proposed method in addressing the challenges of fault diagnosis across diverse operational scenarios.

In our detailed analysis, each signal sample is meticulously composed of 76,800 data points. These samples are normalized to a uniform range between 0 and 1 to ensure consistency across our dataset. To address inherent variability introduced by sample distribution and the initial setup of the neural network, meticulous adjustments were made. We selected softmax regression as our classification method, due to its robustness in handling multi-class classification challenges, which are prevalent in the field of fault diagnosis.

The determination of our network parameters, specifically the regularization parameters λ and α, both set to 1, and the Domain Adaptation (DA) parameter β, set to 1000, was influenced by a combination of theoretical frameworks and best

practices established in previous research. This careful selection process aimed to optimize our model's ability to generalize across varied operational scenarios, ensuring high accuracy and reliability in fault detection and diagnosis.

Our approach was further validated through an extensive review of relevant literature, encompassing both contemporary studies and foundational works in the field. This review helped us to align our methodology with the most effective and recognized standards in fault diagnosis research, as cited in references [9, 33]. By integrating these insights with our empirical observations, we developed a model that not only adheres to the established norms but also pushes the boundaries of what is possible in fault diagnosis through innovative parameter optimization.

4.1.3. Effectiveness Analysis

4.1.3.1. Analysis of Single-source Domain Results

In the context of fault diagnosis under variable working conditions, we conducted experiments transitioning from a single-source domain to a single-target domain. Six sets of experiments were carried out, with the results depicted Fig. 11, representing the averages of 20 random trials. Table 3 provides a detailed overview of the average diagnostic outcomes for each method under six different scenarios.

Compared to the SFDA method, our proposed ESFBDA strategy significantly improved the average diagnostic accuracy by 23.85%, reaching 99.12%. This result highlights limitations in the traditional SFDA method in capturing diagnostic information from multi-condition data adequately.

Fig. 11 clearly shows that the diagnostic results of the SFBDA method are substantially higher than those of the SFDA method, with an improvement of 13.34% according to the results in Table 4. This indicates that introducing joint MMD and Bootstrap methods for DA is highly effective. The combined use of MMD and Bootstrap enhances statistical robustness by allowing random sampling with replacement from the original dataset and in-depth analysis of multiple sub-samples, thus reducing errors due to data variations. However, compared to the ESFBDA proposed, the diagnostic performance of SFBDA remains inferior. Therefore, improving SF indeed plays a crucial role in enhancing diagnostic accuracy.

The RSFDA method emphasizes balancing diversity and consistency, achieving an average accuracy of 93.89%. It focuses on ensuring feature diversity across different domains while emphasizing the consistency of these features among various domains to ensure better generalization of the model in different environments. However, RSFDA mainly emphasizes pre-adaptation of reconstruction coefficient filtering, which may result in specific types of feature loss. On the other hand, ESFBDA reduces redundancy and loss during feature extraction by combining row-column normalization and cosine similarity penalties, thus capturing fault information more accurately. Therefore, ESFBDA outperforms RSFDA in terms of accuracy.

In addition, Table 3 demonstrates that ASFDA achieves an accuracy of 94.71%, which is 4.41% lower than ESFBDA. The difference in performance is attributable to the methodological characteristics of ASFDA, particularly its adaptation strategy in handling domain-specific information when predicting the target domain within a single-source domain experiment. This approach can occasionally result in information confusion among the source domains. On the other hand, ESFBDA uses Bootstrap resampling to optimize MMD for more precise DA, ensuring a more accurate alignment of features between source and target domains.

Moreover, the fault diagnosis results for the SFMCD method are also presented in Fig. 11, achieving an accuracy of 95.38%. This is attributed to the SFMCD method reducing the distribution difference between the source and target domains using Wasserstein distance and adversarial training strategies. Despite its outstanding performance in some aspects, ESFBDA employs Bootstrap resampling optimization MMD for DA, ensuring a more accurate alignment of features between source and target domains. This integrated strategy provides ESFBDA with a solid foundation in DA, balancing feature diversity and domain consistency. Therefore, ESFBDA significantly outperforms SFMCD in terms of accuracy.

Furthermore, the l_1/l_2-SFDA method achieves an average fault diagnosis accuracy of 96.54%, a notable improvement of 7.96 % compared to SFBDA's 88.61%. This result highlights the positive impact of positive-side enhancement on the generalization performance of DA models. While the performance of l_1/l_2-SFDA is slightly below our proposed ESFBDA, it suggests that focusing solely on positive-side features may not fully capture diagnostic features in multi-

condition data. This implies that, apart from emphasizing positive-side features, incorporating Cosine similarity to eliminate similar features is equally vital, thereby enhancing the accuracy of variable working conditions fault diagnosis and model generalization performance.

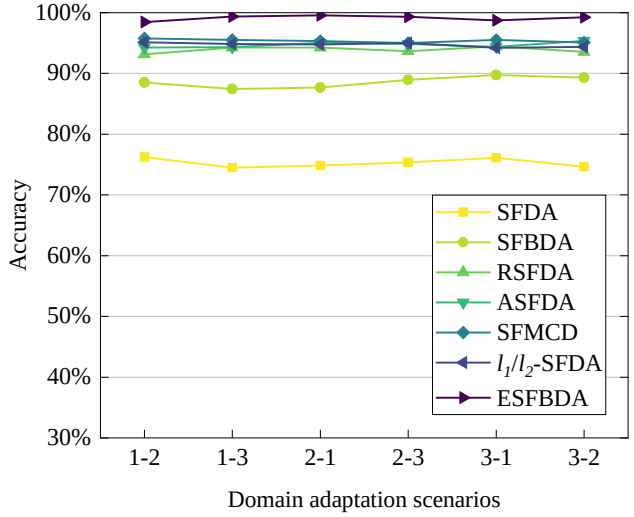

Fig. 11. Variable working conditions fault diagnosis outcomes of the proposed approach versus reference methodologies (sourced from a singular domain).

Table 3. The accuracy comparison results of the method proposed in this paper and various other methods are presented herein (sourced from a singular domain).

Method	Average	SD
SFDA	75.27	0.69
SFBDA	88.61	0.83
RSFDA	93.89	0.47
ASFDA	94.71	0.41
SFMCD	95.38	0.27
l_1/l_2-SFDA	94.72	0.33
ESFBDA	**99.12**	**0.77**

In our comparative analysis, the ESFBDA method demonstrates significant improvements in diagnostic accuracy over traditional approaches, highlighting its effectiveness in overcoming the limitations associated with the normalization process in sparse filtering, especially within high-dimensional and diverse datasets. By integrating row-column normalization and a cosine similarity penalty, our method effectively preserves essential features and captures subtle data variations, which are often lost in traditional normalization processes. This approach ensures a more nuanced understanding and processing of complex data structures, thereby enhancing the model's performance across variable working conditions. The results from our experiments, as illustrated in Fig. 12 and detailed in Table 4, empirically validate this improvement, showcasing ESFBDA's capability to mitigate feature loss and overgeneralization, issues that are prevalent in conventional sparse filtering applications.

To compare the feature extraction capabilities of various methods under unknown conditions, we employed t-distributed stochastic neighbor embedding (t-SNE) [4] for feature dimensionality reduction and visualization. We used the Load 3-2 experiment as an example to depict the features in a three-dimensional space. As illustrated in Fig. 13, the features classified under the SFDA method are intermixed, with substantial overlap in the distribution boundaries of different categories, which compromises classification accuracy. Conversely, while the results from SFBDA, RSFDA, and ASFDA showed a more organized distribution, some confusion still exists. This suggests that traditional SF feature extraction and MMD domain adaptation methods are limited when extracting diagnostic knowledge across conditions. SFMCD and l_1/l_2-SFDA demonstrated relatively better classification performance, albeit with some instances of misclassification. Our proposed method correctly categorized all samples, underscoring its superior fault feature extraction across different speeds. This further validates the efficiency and robustness of our approach in diagnosing faults under variable working conditions.

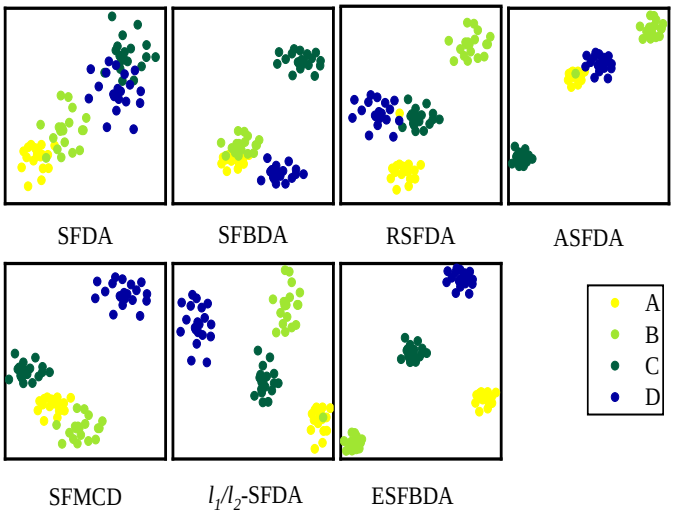

Fig. 13. Visualization results of load 3-2 fault diagnosis experiment.

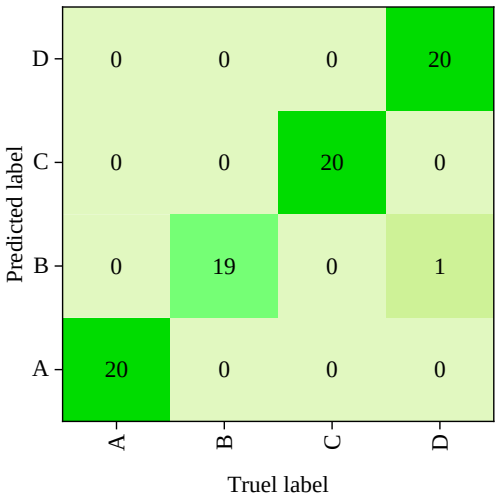

Fig. 14. Confusion matrix illustration of our method in load 3-2 experiment.

Fig. 14 displays the confusion matrix of the ESFBDA method in a load 3-2 experiment. In the confusion matrix, misclassifications between states B and D can be observed, while there are no misclassifications among the other states. This indicates the method's strong performance in classification. Reflecting upon the consistent discussions and findings, the visual interpretation of the confusion matrix accentuates the commendable capability of the proposed method in diagnosing faults across varying conditions.

4.1.3.2. Analysis of Dual-source Domain Results

To further validate the effectiveness of the proposed method, two source domains were selected for predicting the health condition of a target domain. Therefore, there were three tasks in this experiment: 12-3, 13-2, and 23-1. Table 5 lists the diagnostic results for each method.

Table 5. The accuracy comparison results of the method proposed in this paper and various other methods are presented herein (sourced from a dual domain).

Method	Average	SD
SFDA	78.46	0.37
SFBDA	92.01	0.24
RSFDA	94.54	0.65
ASFDA	96.15	0.33
SFMCD	96.66	0.37
l_1/l_2-SFDA	98.34	0.39
ESFBDA	**99.91**	**0.09**

The experimental results are shown in Fig. 15, and the average diagnostic accuracy is listed in Table 5. We can observe that ESFBDA achieves an average fault diagnosis accuracy of 99.91%, which is 0.79% higher than methods that learn fault features from a single domain. Similar improvements are observed with other comparative methods. This suggests that integrating knowledge from two domains into one domain can more effectively leverage multi-source information. Different operating conditions may lead to different data distributions, and by merging these distributions, features, and patterns can be captured more comprehensively. This information fusion provides additional background knowledge, contributing to improved model accuracy.

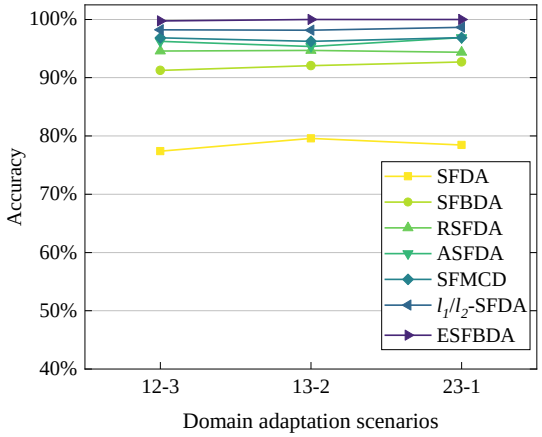

Fig. 15. Variable working conditions fault diagnosis outcomes of the proposed approach versus reference methodologies (sourced from a dual domain).

The t-SNE method was also employed to visualize the diagnostic results of load 23-1. From the graph, it is evident that under the learning of two source domains, all methods exhibit clearer classification, with greater separation between different categories. The method presented in this paper demonstrates exceptional performance in visual classification. It consistently outperforms other methods and achieves highly accurate results. This visual result further emphasizes that by integrating knowledge from two source domains into one domain, it is possible to better distinguish different categories and enhance the model's classification performance. This also demonstrates the unique advantages of the proposed method in addressing variable working conditions diagnostic problems.

Fig. 17 presents the diagnostic results of the ESFBDA method in the Load 23-1 experiment through a confusion matrix. It is evident from the confusion matrix that all four classes A, B, C, and D have been successfully classified with an accuracy of 100%. This result is consistent with the information shown in

Fig. 16. It further emphasizes the efficiency and accuracy of the ESFBDA method in diagnostic tasks.

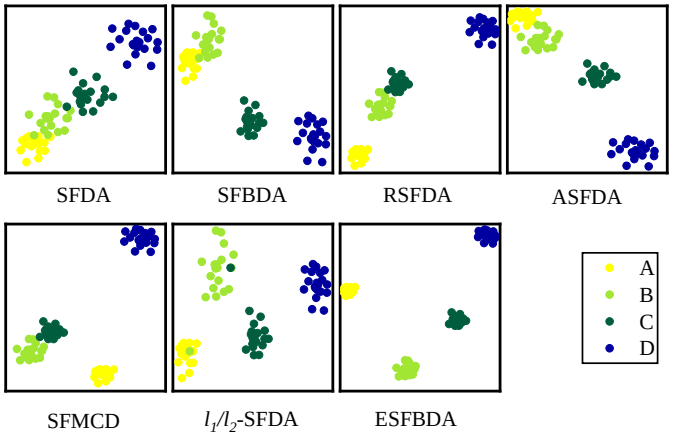

Fig. 16. Variable working conditions diagnostic results of various methods in the experiments for Load 23-1 under small sample conditions.

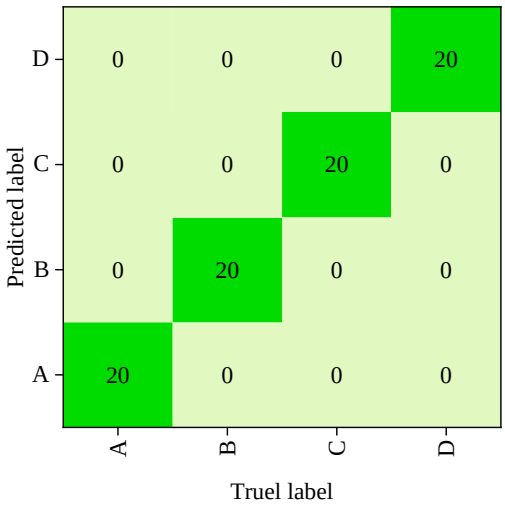

Fig. 17. Confusion matrix illustration of our method in load 23-1 experiment.

4.1.3.3. Analysis of Diagnostic Results with Different Source Domain Sample Sizes

In practical engineering applications, labeled EHA monitoring data is often scarce. Therefore, fault diagnosis models for variable working conditions scenarios need to maintain high diagnostic accuracy even with limited samples. To assess the diagnostic performance of our proposed method under small-sample conditions for unknown conditions, the load 2-3 experiment was selected, and our proposed method, along with six comparative methods, was trained using varying percentages of training samples. Each result is the average of 20 random experiments, and the final diagnostic results are shown in Fig. 18. The training sample ratio represents the percentage of each class's training samples, for example, a 90% training sample ratio means that each class has 90% of the total training samples.

The results demonstrate that as the number of training samples decreases, the diagnostic accuracy of all methods for variable working conditions scenarios decreases to some extent. Our proposed ESFBDA method consistently exhibits the highest diagnostic accuracy under small-sample conditions. As the number of training samples decreases, ESFBDA shows the smallest decline in diagnostic accuracy. Even with only 50% of the training samples, it still achieves a diagnostic accuracy of 95.5% with a standard deviation of only 1.5%. The experiment shows that our method excels in small-sample variable working conditions fault diagnosis.

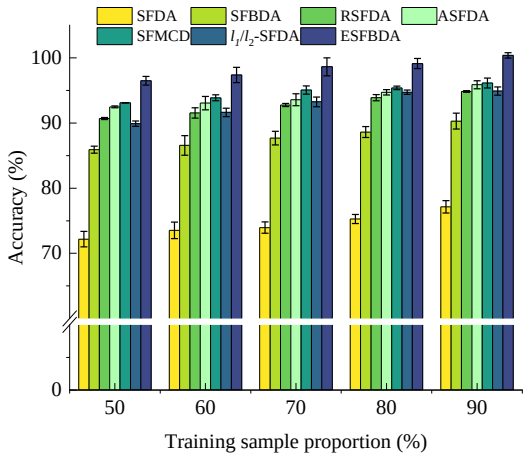

Fig. 18. Variable working conditions diagnostic results of various methods in the experiments for Load 2-3 under small sample conditions.

4.2. Case 2: bearing fault diagnosis

4.2.1. Data Preparation

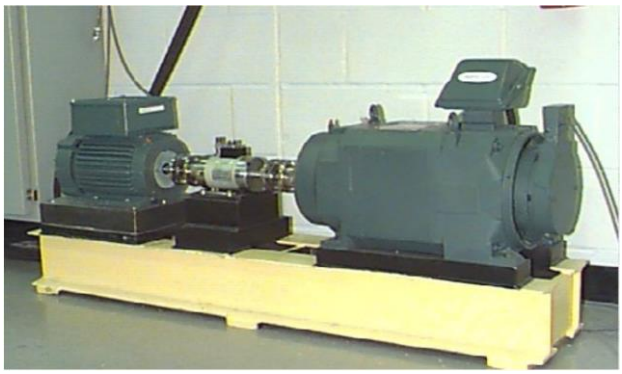

Fig. 18. Case western reserve university bearing data source [23]

To further validate the effectiveness of the ESFBDA method in addressing fault diagnosis under Variable Working Conditions, we utilized a dataset derived from bearing tests, as depicted in Figure 18, featuring the drive end bearing SKF6205-2R [6]. The bearings were artificially damaged on the inner race, ball, and outer race through electrical discharge machining. Vibration signals were collected at a sampling rate of 12 kHz and a rotational speed of 1797 rpm under load conditions of 0, 1, 2, and 3 HP.

The detailed data selected, as outlined in Table 6, considers four health states: (1) Normal Health (NH); (2) Outer Race Fault (OF); (3) Inner Race Fault (IF); and (4) Ball Fault (BF), with a damage diameter of 7 mils.

Table 6. The description of bearing data.

Load (HP)	Fault size (mil)	Fault location
0	7	NH, IF, BF, OF
1		
2		
3		

4.2.3. Effectiveness Analysis

The selection of comparison methods and parameter settings for our analysis adheres to the protocol established in '4.1.2 Comparison Methods and Parameter Selection.' The nine transfer tasks, including task 0-1 which moves from 0hp to 1hp load conditions, rigorously evaluate each method's ability to adapt diagnostic performance across varying operational loads, a fundamental requirement for practical fault identification in industry settings.

Table 7. The accuracy comparison results of the method proposed in this paper and various other methods are presented herein.

Method	Average	SD
SFDA	82.24	2.35
SFBDA	86.74	1.29
RSFDA	94.48	1.27
ASFDA	96.20	0.65
SFMCD	97.05	0.73
l_1/l_2-SFDA	98.49	0.59
ESFBDA	99.52	0.27

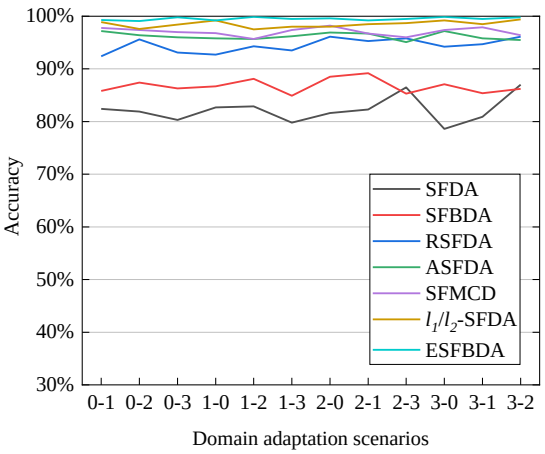

Fig. 19. Variable working conditions fault diagnosis outcomes of the proposed approach versus reference methodologies.

The ESFBDA method, as illustrated in Table 7 and Fig. 19, consistently outperforms competing methods with an impressive average accuracy of 99.52% and a notably low standard deviation of 0.27. This remarkable consistency in achieving high diagnostic accuracy across various operational loads demonstrates the method's robustness and reliability, key for dependable real-time monitoring and fault diagnosis in industrial applications.

Moreover, the method's excellent performance is indicative of its sophisticated ability to capture and classify fault characteristics accurately, regardless of the load transition complexity. This is supported by its leading performance across all individual tasks in the dataset, demonstrating ESFBDA's advanced feature extraction and domain adaptation capabilities that contribute to its high diagnostic accuracy.

In summary, the results solidifies the ESFBDA method's standing as a significant advancement in the domain adaptation landscape for fault diagnosis. The method's robust performance across variable working conditions, demonstrated through comprehensive experimental validation, positions ESFBDA as a leading approach for ensuring the reliability and safety of mechanical systems in the face of diverse operational challenges.

5. Conclusions

This paper introduces a variable working condition fault diagnosis method named ESFBDA, offering higher accuracy in cross-working condition fault diagnosis compared to existing SF-based domain adaptation methods. ESFBDA enhances SF

technology by incorporating l_2 normalization and similarity penalty items, reducing feature loss. Additionally, it optimizes MMD using Bootstrap Resampling for more accurate domain difference assessment. Extensive experiments on an EHA internal leakage fault dataset demonstrate its ability to accurately extract similar features across different working conditions and assess domain differences effectively, thus improving variable working condition fault diagnosis. Specifically, the application of our ESFBDA method to the EHA dataset underscores its significant impact on enhancing fault diagnosis for electro-hydraulic servo systems. This approach not only showcases the method's effectiveness in a real-world context but also illuminates its potential to advance fault diagnosis techniques, ensuring the reliability and safety of such critical systems in the industry.

As for future avenues of exploration, there is potential in amalgamating conditional MMD or multi-kernel MMD with the ESFBDA model. Such integration might unlock further enhancements in the method's overall performance and robustness, solidifying its practical applications in pertinent areas. In addition, future work will critically examine the distinct impacts of column and row normalization in the ESFBDA method, aiming to refine SF for fault diagnosis. This exploration is essential for advancing DA techniques and optimizing performance in varying conditions.

References

1. An Y, Zhang K, Chai Y, Liu Q, Huang X. Domain adaptation network base on contrastive learning for bearings fault diagnosis under variable working conditions. Expert Systems with Applications. 2023;212:118802. https://doi.org/10.1016/j.eswa.2022.118802
2. Azamfar M, Singh J, Li X, Lee J. Cross-domain gearbox diagnostics under variable working conditions with deep convolutional transfer learning. Journal of Vibration and Control. 2021;27(7-8):854-864. https://doi.org/10.1177/1077546320933793
3. Bao H, Yan Z, Ji S, Wang J, Jia S, Zhang G, et al. An enhanced sparse filtering method for transfer fault diagnosis using maximum classifier discrepancy. Measurement Science and Technology. 2021;32(8):085105. https://doi.org/10.1088/1361-6501/abe56f
4. Belkina AC, Ciccolella CO, Anno R, Halpert R, Spidlen J, Snyder-Cappione JE. Automated optimized parameters for T-distributed stochastic neighbor embedding improve visualization and analysis of large datasets. Nature communications. 2019;10(1):5415. https://doi.org/10.1038/s41467-019-13055-y
5. Borgwardt KM, Gretton A, Rasch MJ, Kriegel H-P, Schölkopf B, Smola AJ. Integrating structured biological data by kernel maximum mean discrepancy. Bioinformatics. 2006;22(14):e49-e57. https://doi.org/10.1093/bioinformatics/btl242
6. Center BD. Case western reserve university bearing data [Internet]. Cleveland, Ohio, U.S. Case School of Engineering. Available from: http://csegroups, case. ed./bearingdatacenter/pages/down-loaddata-file
7. Chopra P, Yadav SK. Restricted Boltzmann machine and softmax regression for fault detection and classification. Complex & Intelligent Systems. 2018;4:67-77. https://doi.org/10.1007/s40747-017-0054-8
8. Ding Y, Jia M, Zhuang J, Cao Y, Zhao X, Lee C-G. Deep imbalanced domain adaptation for transfer learning fault diagnosis of bearings under multiple working conditions. Reliability Engineering & System Safety. 2023;230:108890. https://doi.org/10.1016/j.ress.2022.108890
9. Gould NI, Porcelli M, Toint PL. Updating the regularization parameter in the adaptive cubic regularization algorithm. Computational optimization and applications. 2012;53:1-22. https://doi.org/10.1007/s10589-011-9446-7
10. Griffin D, Lim J. Signal estimation from modified short-time Fourier transform. IEEE Transactions on acoustics, speech, and signal processing. 1984;32(2):236-243. https://doi.org/10.1109/TASSP.1984.1164317
11. Han C, Lei Y, Xie Y, Zhou D, Gong M. Visual domain adaptation based on modified A− distance and sparse filtering. Pattern Recognition. 2020;104:107254. https://doi.org/10.1016/j.patcog.2020.107254
12. He Y-L, Yan X, Zhu Q-X. Novel pattern recognition using bootstrap-based discriminant locality-preserving projection and its application to fault diagnosis. Industrial & Engineering Chemistry Research. 2019;58(38):17906-17917. https://doi.org/10.1021/acs.iecr.9b03752
13. Ji S, Han B, Zhang Z, Wang J, Lu B, Yang J, et al. Parallel sparse filtering for intelligent fault diagnosis using acoustic signal processing. Neurocomputing. 2021;462:466-477. https://doi.org/10.1016/j.neucom.2021.08.049
14. Jiang M, Liang Y, Feng X, Fan X, Pei Z, Xue Y, et al. Text classification based on deep belief network and softmax regression. Neural

Computing and Applications. 2018;29:61-70. https://doi.org/10.1007/s00521-016-2401-x

15. Kouw WM, Loog M. A review of domain adaptation without target labels. IEEE transactions on pattern analysis and machine intelligence. 2019;43(3):766-785. https://doi.org/10.1109/TPAMI.2019.2945942
16. Li W, Huang R, Li J, Liao Y, Chen Z, He G, et al. A perspective survey on deep transfer learning for fault diagnosis in industrial scenarios: Theories, applications and challenges. Mechanical Systems and Signal Processing. 2022;167:108487. https://doi.org/10.1016/j.ymssp.2021.108487
17. Li X, Zhang W, Ding Q. Understanding and improving deep learning-based rolling bearing fault diagnosis with attention mechanism. Signal processing. 2019;161:136-154. https://doi.org/10.1016/j.sigpro.2019.03.019
18. Ma Y, Shan C, Gao J, Chen H. Multiple health indicators fusion-based health prognostic for lithium-ion battery using transfer learning and hybrid deep learning method. Reliability Engineering & System Safety. 2023;229:108818. https://doi.org/10.1016/j.ress.2022.108818
19. Pan SJ, Tsang IW, Kwok JT, Yang Q. Domain adaptation via transfer component analysis. IEEE transactions on neural networks. 2010;22(2):199-210. https://doi.org/10.1109/TNN.2010.2091281
20. Qian Q, Wang Y, Zhang T, Qin Y. Maximum mean square discrepancy: a new discrepancy representation metric for mechanical fault transfer diagnosis. Knowledge-Based Systems. 2023;276:110748. https://doi.org/10.1016/j.knosys.2023.110748
21. Schwendemann S, Amjad Z, Sikora A. Bearing fault diagnosis with intermediate domain based layered maximum mean discrepancy: A new transfer learning approach. Engineering Applications of Artificial Intelligence. 2021;105:104415. https://doi.org/10.1016/j.engappai.2021.104415
22. Shi Y, Deng A, Ding X, Zhang S, Xu S, Li J. Multisource domain factorization network for cross-domain fault diagnosis of rotating machinery: An unsupervised multisource domain adaptation method. Mechanical Systems and Signal Processing. 2022;164:108219. https://doi.org/10.1016/j.ymssp.2021.108219
23. Smith WA, Randall RB. Rolling element bearing diagnostics using the Case Western Reserve University data: A benchmark study. Mechanical systems and signal processing. 2015;64:100-131. https://doi.org/10.1016/j.ymssp.2015.04.021
24. Wang C, Zhu G, Liu T, Xie Y, Zhang D. A sub-domain adaptive transfer learning base on residual network for bearing fault diagnosis. Journal of Vibration and Control. 2023;29(1-2):105-117. https://doi.org/10.1177/10775463211042976
25. Wang J, Ji S, Han B, Bao H. Intelligent fault diagnosis for rotating machinery using L1/2-SF under variable rotational speed. Proceedings of the Institution of Mechanical Engineers, Part D: Journal of Automobile Engineering. 2021;235(5):1409-1422. https://doi.org/10.1177/0954407020964625
26. Wang M, Deng W. Deep visual domain adaptation: A survey. Neurocomputing. 2018;312:135-153. https://doi.org/10.1016/j.neucom.2018.05.083
27. Yao Y, Wang H. Optimal subsampling for softmax regression. Statistical Papers. 2019;60:585-599. https://doi.org/10.1007/s00362-018-01068-6
28. Zennaro FM, Chen K. Towards understanding sparse filtering: A theoretical perspective. Neural Networks. 2018;98:154-177. https://doi.org/10.1016/j.neunet.2017.11.010
29. Zhang G, Han B, Li S, Wang J, Wang X. General normalized maximum mean discrepancy: intelligent fault identification method for bearings and gears under unstable conditions. Measurement Science and Technology. 2021;32(10):104001. https://doi.org/10.1088/1361-6501/abf3fb
30. Zhang Y, Ji J, Ma B. Reciprocating compressor fault diagnosis using an optimized convolutional deep belief network. Journal of Vibration and Control. 2020;26(17-18):1538-1548. https://doi.org/10.1177/1077546319900115
31. Zhang Y, Ji J, Ren Z, Ni Q, Gu F, Feng K, et al. Digital twin-driven partial domain adaptation network for intelligent fault diagnosis of rolling bearing. Reliability Engineering & System Safety. 2023;234:109186. https://doi.org/10.1016/j.ress.2023.109186
32. Zhang Y, Ren Z, Zhou S, Feng K, Yu K, Liu Z. Supervised contrastive learning-based domain adaptation network for intelligent unsupervised fault diagnosis of rolling bearing. IEEE/ASME Transactions on Mechatronics. 2022;27(6):5371-5380. https://doi.org/10.1109/TMECH.2022.3179289
33. Zhang Z, Huang W, Liao Y, Song Z, Shi J, Jiang X, et al. Bearing fault diagnosis via generalized logarithm sparse regularization. Mechanical Systems and Signal Processing. 2022;167:108576. https://doi.org/10.1016/j.ymssp.2021.108576

34. Zhang Z, Yang Q. Unsupervised feature learning with reconstruction sparse filtering for intelligent fault diagnosis of rotating machinery. Applied Soft Computing. 2022;115:108207. https://doi.org/10.1016/j.asoc.2021.108207
35. Zhou Z, Chen W, Yang C. Adaptive range selection for parameter optimization of VMD algorithm in rolling bearing fault diagnosis under strong background noise. Journal of Mechanical Science and Technology. 2023;37(11):5759-5773. https://doi.org/10.1007/s12206-023-1015-3